Optics and Lasers in Engineering 47 (2009) 390–397

Contents lists available at ScienceDirect

Optics and Lasers in Engineering

journal homepage: www.elsevier.com/locate/optlaseng

Study of the deformation characteristics of window security film by digital image correlation techniques

Wim Van Paepegem [a,*], Assen A. Shulev [b], Ilia R. Roussev [b], Stijn De Pauw [a], Joris Degrieck [a], Ventseslav C. Sainov [c]

[a] Department of Mechanical Construction and Production, Ghent University, Sint-Pietersnieuwstraat 41, 9000 Gent, Belgium
[b] Institute of Mechanics, Bulgarian Academy of Sciences, Bl. 4, Acad. G. Bonchev St., 1113 Sofia, Bulgaria
[c] Central Laboratory of Optical Storage and Processing of Information, Bulgarian Academy of Sciences, Bl. 101, Acad. G. Bonchev St., P.O. Box 95, 1113 Sofia, Bulgaria

ARTICLE INFO

Available online 22 April 2008

Keywords:
Digital speckle photography
Digital image correlation
Sub-pixel accuracy
Window security film

ABSTRACT

This paper presents a speckle-displacement measurement technique based on the digital image correlation to study the notch sensitivity and crack bridging of window security film. It is used to protect existing glazing against hurricanes, blast and terrorist explosions. The window security film is laminated to the interior side of the glass window by means of a special adhesive. When the glass is breaking, the window film keeps all glass fragments together.

The proposed sub-pixel registration of the displacement field is achieved using a calculation technique based on the centre of mass localization of the complex spectrum. This approach increases the computational efficiency for displacements smaller than one pixel and performs with high precision when optimal values of the input correlation parameters are used. In order to achieve a high accuracy of the algorithm, optimization of these input image correlation parameters is offered. For larger displacements an iterative procedure which preserves the precision is successfully implemented.

The speckle pattern is created by small white dots sprayed on the previously black painted film surface. As a result, white light illumination can be used which significantly simplifies the experiments.

1. Introduction

Speckle photography is one of the most popular and promising non-destructive techniques for small displacement, strain and rotation measurements [1–6]. In addition to the simplicity and reliability of in-plane measurements, recently out-of-plane motion measurement has been successfully applied [7]. Its ability to provide precise and full field information, combined with a low vibration sensitivity and high measurement range, makes it suitable for investigations of all kinds of materials. In the past two decades, many digital image correlation (DIC) techniques have been developed to improve the accuracy of the speckle photography approach. DIC is based upon comparing numerically two images of the specimen surface in the undeformed and deformed states assuming that the speckle structure remains almost unchanged during the deformation process. A significant progress of the measurement accuracy has been recently achieved by many different DIC algorithms. The main reason is that a sub-pixel registration has been proposed and successfully applied to study the displacement and strain fields. Some DIC algorithms rely on the intensity interpolation [8,9], others on Newton–Raphson iteration [10,11], curve-fitting or interpolation of the correlation coefficients [12,13], optical flow method [14,15], complex spectrum [16], genetic and neural network methods [17,18]. The precision and sensitivity of these algorithms range from 0.5 to 0.01 pixels. Some advantages in the accuracy of the Newton–Raphson method over the curve-fitting of the correlation coefficients and optical flow methods, which are the most commonly used, have been emphasized in the literature [19]. It is also relevant to remark that most DIC techniques cannot obtain directly the strain fields, as the Newton–Raphson method, which could be of interest in some cases. Nevertheless, the strain fields can be calculated by numerical differentiation of the previously obtained displacement fields. On the other hand, knowing the displacement fields can be an advantage when investigating the dynamics of the processes, for example, the velocity of crack and fracture propagation.

Other important features of all these algorithms are their simplicity and computational efficiency. In many cases a suitable compromise between the accuracy, computational efficiency and simplicity should be made. The right choice usually is a difficult task, which depends mainly on the specificity of the investigated object.

* Corresponding author. Tel./fax: +32 9 264 35 87.
E-mail address: Wim.VanPaepegem@UGent.be (W. Van Paepegem).

0143-8166/$ - see front matter © 2008 Elsevier Ltd. All rights reserved.
doi:10.1016/j.optlaseng.2008.03.005

In this paper, we present a straightforward and relatively fast technique for DIC with sub-pixel accuracy. It is applied for the investigation of the notch sensitivity, tear resistance and crack bridging of a window security film in its interaction with glass.

2. Algorithm

Two speckle patterns of the investigated object are captured by a digital camera, one before and one after a certain deformation. These two images are segmented in small sub-images typically of $(2M+1)\times(2M+1)$ pixels so that the displacement in each sub-image can be treated as a simple uniform translation. The corresponding sub-image pairs extracted from both states of the specimen are processed, and the displacement vector is calculated by the complex spectrum method described in [16].

Let $h_1(x, y)$ and $h_2(x, y)$ be the corresponding sub-image pairs extracted from both states and analysed by a two-step fast-Fourier transform. The function measuring the correlation between these two sub-images has the following form:

$$C(x,y) = F^{-1}\left\{\frac{F\{h_1(x,y)\}F\{h_2(x,y)\}^*}{|F\{h_1(x,y)\}F\{h_2(x,y)\}|^{1-\alpha}}\right\}, \quad (1)$$

where F and F^{-1} are the direct and inverse two-dimensional Fourier transforms, respectively, * denotes complex conjugate, and α is an appropriate constant $(0<\alpha<1)$. Actually α represents to what extent the spectral amplitudes of both sub-images contribute to the joint correlation. When $\alpha=0$ only the spectral phases of the two sub-images take part in the correlation which is equivalent to phase-only cross correlation between these images. When $\alpha=1$ the spectral amplitudes and phases are equally presented in the correlation which is equivalent to a cross correlation between the two sub-images. The normalized correlation functions of three sub-image pairs corresponding to three different displacements and for three values of α are illustrated in Fig. 1.

The local displacement vector is determined by the position of the sharpest correlation peak with respect to the origin of the coordinate system. Evidently, the quality of the correlation peak depends on α and on the displacement which can be seen in Fig. 1. When α is small the correlation peak is narrow while it is broad when α is large. If the displacement is close to half of the sub-image size M, the correlation peak is smeared out because of non-overlapping between identical parts in the two sub-images. This non-overlapping leads to random fluctuations in the correlation function which worsens the correlation peak quality and thus increases the possibility for wrong detection of its exact position.

The position of the correlation peak is calculated with integer pixel accuracy. So the displacement accuracy is restricted by the pixel size of the camera sensor. To overcome this disadvantage and to achieve a higher local displacement resolution, a sub-pixel analysis of the peak position is required. Many different techniques, such as a bi-parabolic least-square fitting near the signal peak [16], two-dimensional quadratic surface fitting [12], or expanding the discrete correlation function in terms of a Fourier series around the discrete correlation peak [20] are used.

Here we discuss a straightforward and faster sub-pixel localization of the correlation peak, based on the assumption that its exact position coincides with the centre of mass of the signal peak [21]. The centre of mass can be presented as

$$(x_{cm}, y_{cm}) = \frac{\sum_{x,y} C(x,y)(x,y)}{\sum_{x,y} C(x,y)}, \quad (2)$$

where (x_{cm}, y_{cm}) is a vector with coordinates x_{cm} and y_{cm} corresponding to the centre of mass position, $C(x,y)$ is the correlation function presented by Eq. (1), and (x, y) is a vector

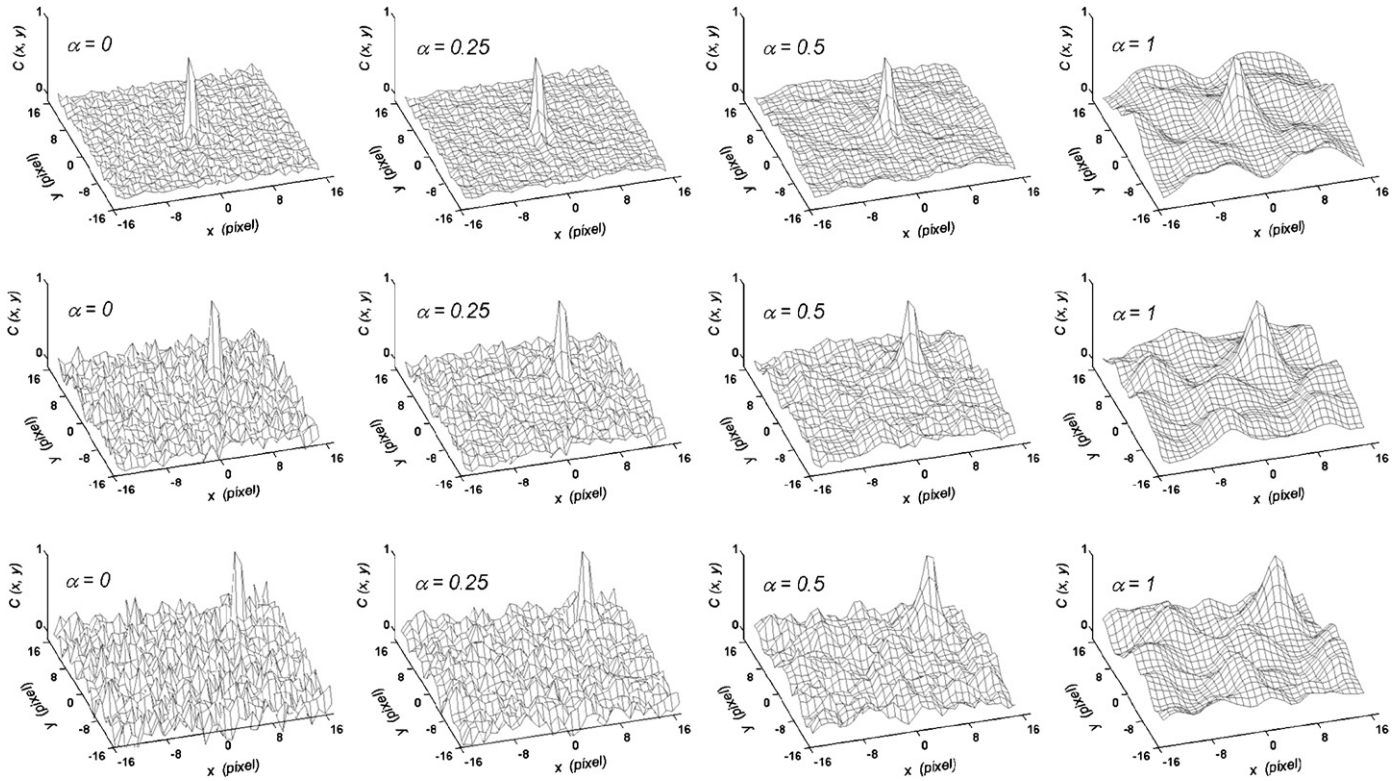

Fig. 1. Normalized correlation functions for three displacements (x,y): first row (0.42, 0.42) pixels, second row (5.43, 5.43) pixels, third row (9.42, 9.42) pixels. The value of α varies through the columns: first column $\alpha=0$, second column $\alpha=0.5$, third column $\alpha=1$.

with integer coordinates x and y corresponding to the nearest neighbouring pixels to the correlation peak.

Apparently the sub-pixel displacement estimation depends on the correlation peak quality and thus on the parameter α. Therefore, it is of great importance to find the optimal value of α in order to achieve high precision of the calculated displacements. Since we use the centre of mass approach for an $m \times m$ pixel array the best performance could be expected when the correlation peak is concentrated over this array. It has been experimentally verified that a 3×3 array for the centre of mass estimation gives best performance and using bigger arrays does not improve the end result even for larger values of α.

From computational point of view the number of numerical operations required to calculate the centre of mass of an $m \times m$ array is $2m^2-m+1$. In our approach to estimate sub-pixel displacements, $m = 3$ leads to only 16 arithmetic operations. For instance the number of necessary calculations for bi-parabolic fitting is much larger.

3. Sub-pixel accuracy evaluation

The sub-pixel registration precision and sensitivity depend not only on the calculation method but also on the imaging device, optical distortions, optical set-up, and the surface pattern [22]. Some DIC algorithms show nice results on simulated data, but perform not so satisfactorily on real experimental data. The reasons are that real data are quantized, affected by electronic noise and environmental disturbances such as vibrations and air turbulence. That is why we want to deal with real experimental data in order to validate the precision of the above-proposed method and presented results.

To evaluate its precision, a simple translational experiment was made. A specimen with speckle pattern surface was translated at an increment step of 1 μm by means of a manual micro-positioning stage with an error of 0.1 μm. The optical magnification was 0.256 and the CCD-camera pixel size was 6.7 μm. This means that each increment step corresponds to 0.038 pixels displacement with an error of ± 0.004 pixel in the image plane. This error is much smaller than the accuracy which can be presented by any DIC method on real data. So this error cannot affect our further considerations.

The displacements were calculated at an image area of (300×300) pixels with correlation sub-image sizes of 17×17, 33×33, and 65×65 pixels. The number N of the calculated displacements from different sub-image pairs was 81.

Two major error components associated with the sub-pixel registration algorithms are: the systematic error E_{sys} (i.e. mean bias error) and the standard deviation error σ. The systematic error is defined as

$$E_{sys} = D_{mean} - D_{defined}, \tag{3}$$

where $D_{mean} = \sum_{i=1}^{N} D_i/N$ represents the mean of N calculated displacements and $D_{defined}$ is the pre-defined displacement. The standard deviation error has a certain relationship with the random error and can be defined as

$$\sigma = \left(\frac{1}{N-1} \sum_{i=1}^{N} (D_{mean} - D_{defined})^2 \right)^{1/2}. \tag{4}$$

To improve the algorithm accuracy, the optimal value of the initial parameter α should be found. For that purpose, different values of the parameter α were tested. Best coincidence of the calculated results with the real pre-defined displacements for a correlation sub-image size of 33×33 pixels was achieved for $\alpha = 0.14$, which can be seen in Fig. 2 presenting the systematic error (left) and the standard deviation (right) as a function of the actual pre-defined sub-pixel displacement and the parameter α.

In order to maintain the high accuracy of the proposed algorithm, the initial parameter α should vary with respect to the chosen sub-image correlation window size. For example, the best match between the calculated results and pre-defined displacements for a sub-image correlation window of 17×17 pixels is achieved when $\alpha = 0.10$, while for a sub-image correlation window of 65×65 pixels, the best match is reached when $\alpha = 0.16$. In Fig. 3, the variation of the calculated systematic error and standard deviation with the pre-defined displacement is shown for the different sub-image correlation window sizes of 17×17, 33×33 and 65×65 pixels. The corresponding optimal values of the parameter α were 0.10, 0.14 and 0.16, respectively.

For the small sub-image correlation windows, the standard deviation takes higher values than for the larger sub-image correlation windows, which is mostly due to the camera noise. So this fact should not be neglected when choosing the sub-image correlation size. In many practical tasks, a small correlation window is not required so this disadvantage could be avoided.

As we mentioned in the previous section, the quality of the correlation peak depends also on the displacement. The correlation peak quality decreases with the displacement increment, affecting the accuracy of the sub-pixel estimation. Using the centre of mass approach for large displacements, the accuracy can

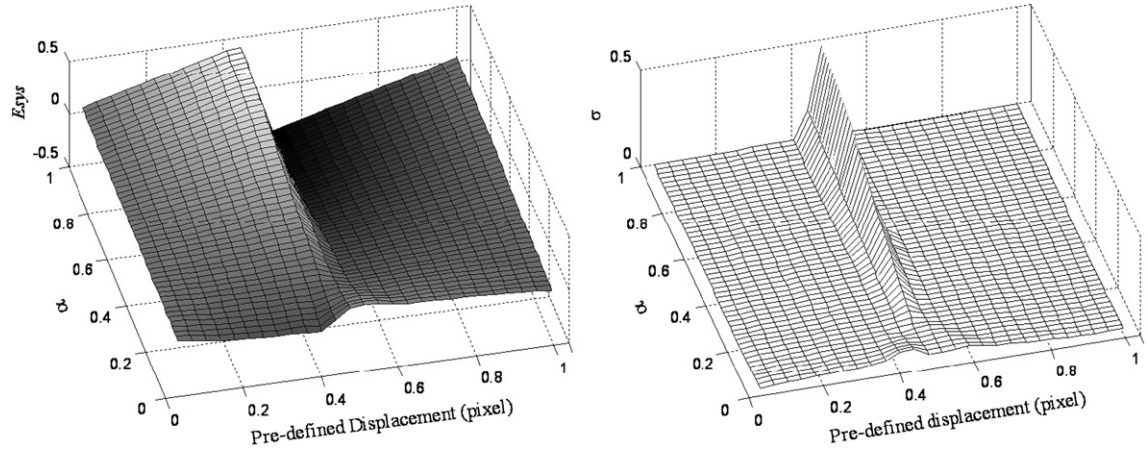

Fig. 2. Systematic error (left) and standard deviation (right) obtained with a sub-image correlation window of 33×33 pixels for rigid body translation over 0–1 pixel displacement and for α varying from 0 to 1.

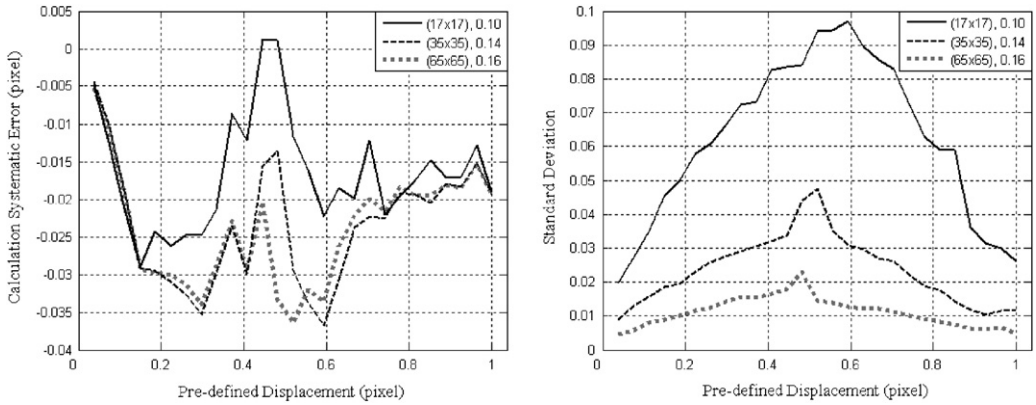

Fig. 3. Systematic error (left) and standard deviation (right) obtained with sub-image correlation windows of 17×17, 33×33 and 65×65 pixels for the optimal values of $\alpha = 0.10, 0.14, 0.16$, respectively. The rigid body pre-defined translation is from 0 to 1 pixel.

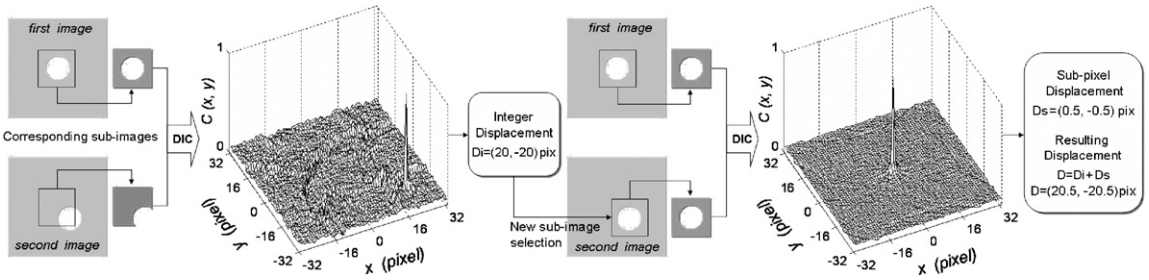

Fig. 4. Graphical presentation of the iterative procedure for large pixel displacements. The size of the sub-images is (65×65) pixels.

drop more than twice, but this is also valid for most of the existing sub-pixel approximations of the correlation peak.

To overcome this disadvantage, we propose an iterative procedure. First the correlation of two sub-images with corresponding position in the two speckle patterns is calculated, and the correlation peak is searched. The displacement from its original position is retrieved with integer pixel accuracy, for simplicity we will call it integer displacement. If the displacement is not zero, then another sub-image from the second image is taken according to the calculated displacement. This routine is similar to simply shifting of the two images toward each other with known shift equal to the calculated displacement. In this way a maximum overlapping between identical parts in the two sub-images is provided. Next the correlation is calculated again. If the integer displacement is then zero, the sub-pixel displacement can be estimated by the centre of mass approach. The resulting displacement is the sum of the integer and sub-pixel displacements. A graphical presentation of this iterative procedure is shown in Fig. 4. The direct application of this iterative procedure will increase the computational time twice. However if the integer displacement can be predicted somehow, e.g. from previous results, then the sub-pixel accuracy is realized at the first iteration and the global computational efficiency does not suffer too much. This is possible when displacement variations are smooth, since the integer displacements are the same for large regions. Sometimes the integer displacement can be different from zero after the second correlation which can occur with partially correlated speckle patterns and/or speckle displacements larger than half of the sub-image size. In this case the procedure is repeated again but with a larger sub-image size. Another advantage of this iterative procedure when measuring large displacements is that the sub-image size during the second correlation can be reduced to a preferable value.

This iterative procedure was tested and successfully applied to study the mechanical behaviour and properties of the window security film (Fig. 5).

4. Investigated object

In a lot of large buildings, the float glass in the windows is retrofitted with a safety and security film, which is applied to the interior side of the glass window by means of a pressure sensitive adhesive (PSA). This polyester film prevents the glass fragments from being shattered around, if the glass window is impacted by a hurricane, a bomb blast, a person falling in the window, etc. The polyester film has a very large deformation capability and keeps all broken glass pieces together. The mechanisms of these polyester films are not fully understood yet, and therefore additional mechanical tests are needed.

In this paper the notch sensitivity and crack bridging of the polyester film were investigated by means of properly designed tensile tests. No attempt is made here to interpret the physical mechanisms of tearing and crack bridging of the film, as this is beyond the scope of this paper and falls within the proprietary of the company supporting this research. The discussion below is limited to the DIC results.

5. Experimental results

The surface of a continuous layer of the window film has been sprayed with a matt black paint, followed by a very fine dust of matt white paint. The chosen paint adheres to the film surface providing a stable non-flaking thin layer which does not change the properties of the window film. The speckle pattern was

Fig. 5. Stacking of polyester film on float glass (left) and impact of window with security film (right).

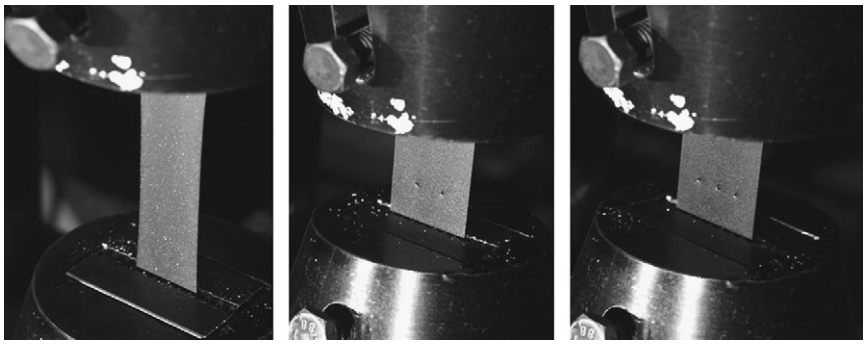

Fig. 6. Tensile tests on window film without holes (left), with two holes (middle), and with three holes (right).

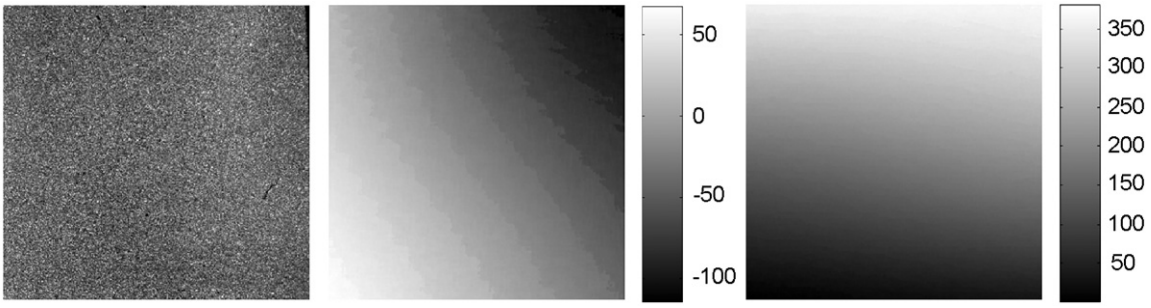

Fig. 7. Displacement fields for the specimen at a load increment of 50 N (from 200 to 250 N). First image presents the original speckle pattern. The second and third images present the displacement fields in x (horizontal) and y (vertical) direction, respectively, in microns, as indicated on the halftone bars.

generated by illuminating the film surface with two strong white light beams, symmetrical in respect to the optical axis (normal to the surface). Usually the speckle patterns produced in such manner are preferred due to the simplicity of the optical set-up, large speckle size variation, and the ability to process images with large deformations without loss of speckle correlation.

First, the polyester film was tested alone, without any interaction with the glass pane. Static tensile tests were performed on strips of the polyester film, both with holes and without holes, to test the notch sensitivity of the film (Fig. 6).

All experiments were performed with an optical magnification of 0.28 and Hitachi P110 camera with a CCD-array of 1024×1024 square pixels with size 6.7 μm and 8 bits quantization. Therefore, a displacement of one pixel corresponded to 23.8 μm displacement in the object plane. To illuminate the object two slide projectors with 100 W halogen bulbs and integrated infrared filters reducing the unwanted thermal spectrum were used. The specimen was stretched by means of a specially designed low vibration hydraulic loading device. The correlation procedure was applied for each pixel of the pattern using square sub-image pairs of size 33×33 pixels.

Fig. 7 shows the correlated displacement fields for a polyester film without holes, and Fig. 8—with one, two and three holes. The first images in both figures show the speckle pattern as it was recorded with the digital CCD camera. Frames were recorded with a speed of 4 fps during the static tensile tests. The second and third columns show the x-displacement (horizontal width direction) and y-displacement (vertical length direction) for an increment of 50 N in load. The displacement fields are shown in grey level scale corresponding to the micrometers as indicated on the halftone bars.

Next, to test the crack bridging of the polyester film and the effect of the PSA, we have designed a tensile experimental set-up, shown in Fig. 9. To simulate a real crack, a rectangular glass plate is raw cut into two halves. The two edges of the crack are not polished or treated otherwise. Next the two halves are aligned again, whether or not with a small distance in between. A polyester film is laminated to both sides of the glass plates with a PSA. Then the two glass plates are pulled away from each other and the in-plane strain field in the film is observed. The strains on the glass surface are small, but in between the two glass plates, the film can stretch very large. In this way, we learn a lot about the "crack bridging" mechanisms of the film.

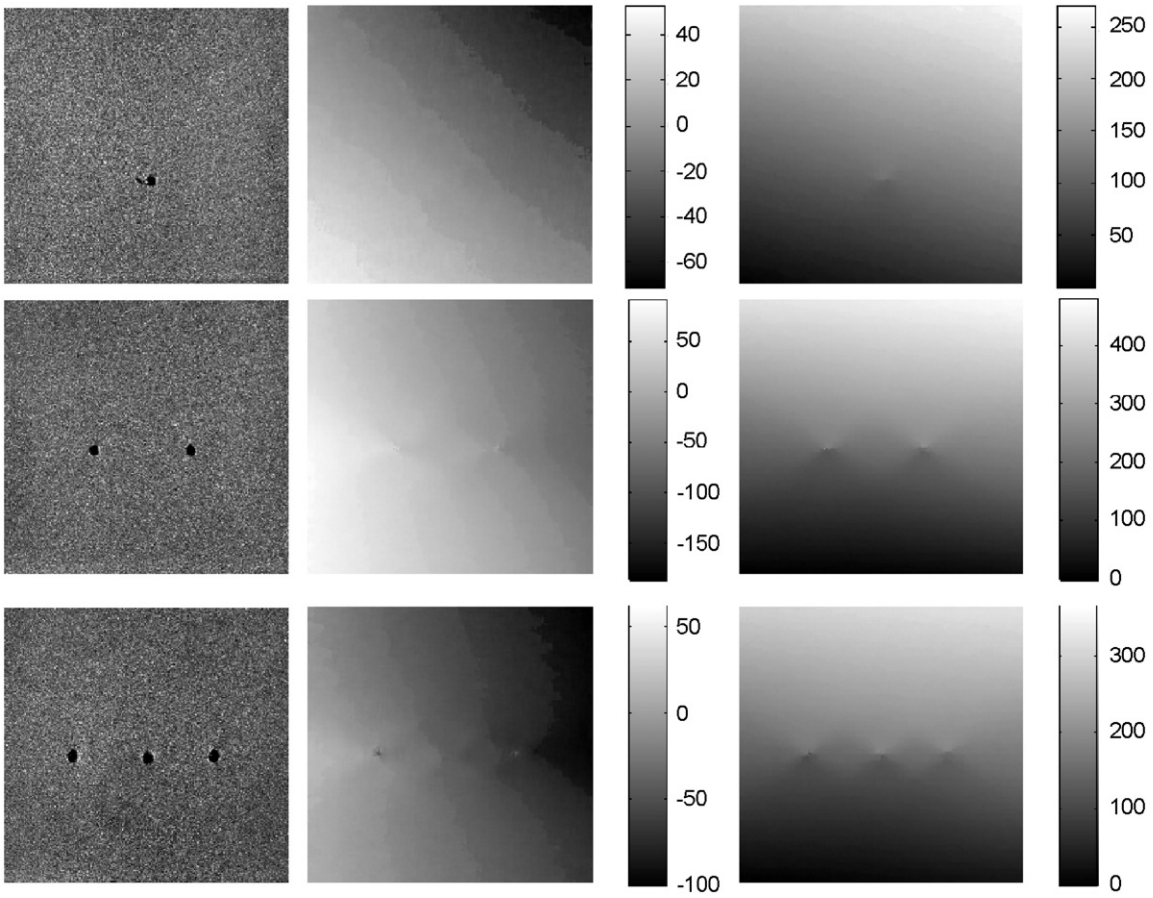

Fig. 8. Displacement fields for specimens with different number of holes at a load increment of 50 N (from 200 to 250 N). In the first column the original speckle patterns for the three cases are shown. The second and third columns present the displacement fields in *x* (horizontal) and *y* (vertical) direction, respectively, in microns, as indicated on the halftone bars.

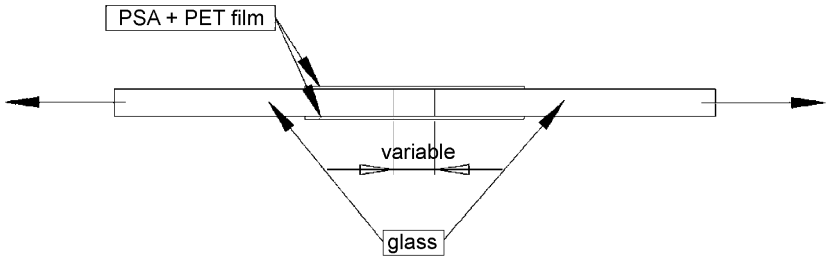

Fig. 9. Schematic of the tensile test on two glass fragments with window security film.

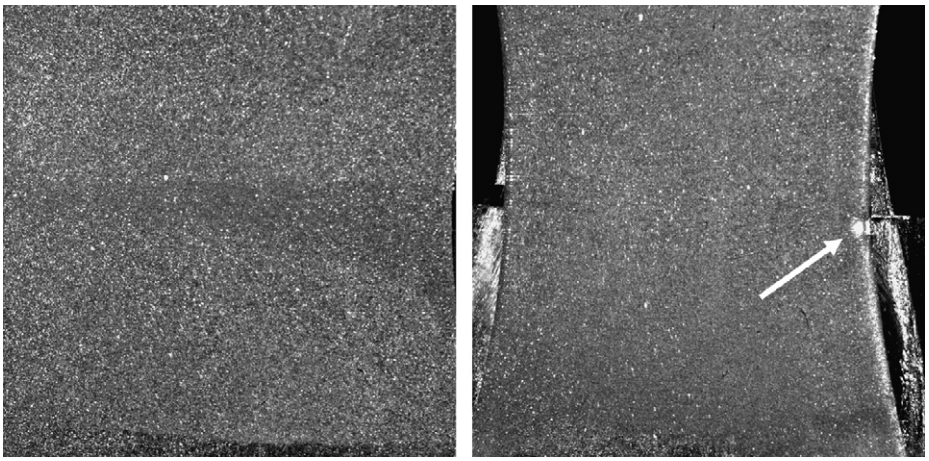

Fig. 10. Corresponding speckle pattern images taken at point A (left) when debonding starts, and point B (right) when tearing of film starts.

In the experiments discussed below, the initial intermediate distance between the two glass plates was zero. One of the two polyester films was sprayed again with a speckle pattern and the investigated surface area of the polyester film on this side was about $30 \times 30\,mm^2$, with the raw cut crack between the two glass plates in the centre of the images. During the tensile tests 1000 frames (4 frames per second) were captured and the measured load (in Newtons) for each frame was recorded. Fig. 10 shows the speckle images at two important moments in time: point *A* (left) where the film starts to debond from the lower glass plate, and point *B* (right) where the film starts to tear apart from the rightmost side (indicated by the white arrow). It can be clearly seen from the right picture that the lower glass plate is clamped and its edge is visible in the horizontal centre of the image, while the upper glass plate has already moved outside the camera's view. In the background, the film that is laminated on the backside of the glass plates is also visible. Both films show very large necking and plastic deformation.

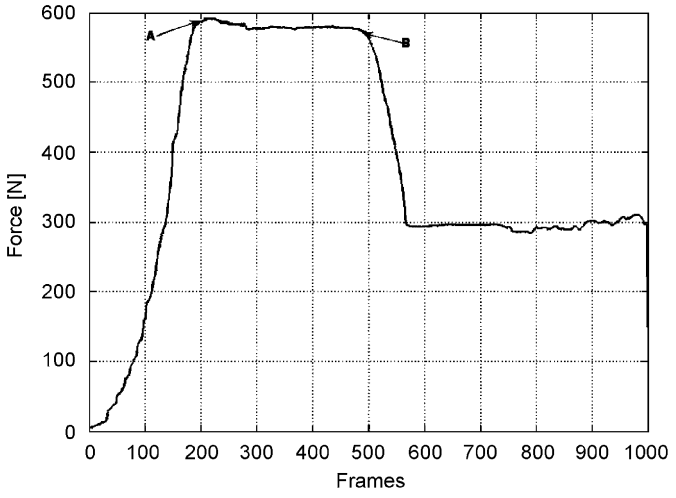

Fig. 11. Plot of the force (in Newtons) vs. frame number (at the frequency of 4 fps) for the specimen of Fig. 9. A labels the beginning of the debonding process; B labels the moment of the beginning of tearing.

Of course, as soon as one of the two films starts tearing apart, the force drops to about half its value. This is confirmed by Fig. 11 that presents a plot of the relation between the applied force and the frames number (respectively time) from a single experiment. The moment of first debonding and tearing of the film are labelled with *A* and *B* on the plot. As soon as the film in front has been torn completely, the force drops to about half its value and the film at the backside keeps stretching. During plastic stretching of the films, the force is almost constant.

In Fig. 12 two images from the experimental set-up are shown close to final failure. One of the two films has been torn apart completely, while the other film is bridging the crack over a very large distance. The film is also necking over a large distance on the glass plates itself.

Two successive frames, captured at the moment *A*, are processed with the proposed algorithm and the obtained displacement fields in *x* and *y* directions, respectively, are shown in Fig. 13. The same calculation was made for the moment *B*, and the results are presented in Fig. 14. Only the selected area in the white rectangle has been processed, because outside of its borders parts of the background, rear film, and glass could be seen which are not interesting for the investigation.

6. Conclusions

A straightforward displacement measurement technique based on the DIC has been proposed. The sub-pixel resolution routine relies on the centre of mass estimation of the correlation peak. Experimental optimization of the correlation parameter α has been proposed to achieve maximum measurement accuracy for

Fig. 12. Tensile test on glass with window film shows the crack bridging capability of the window film.

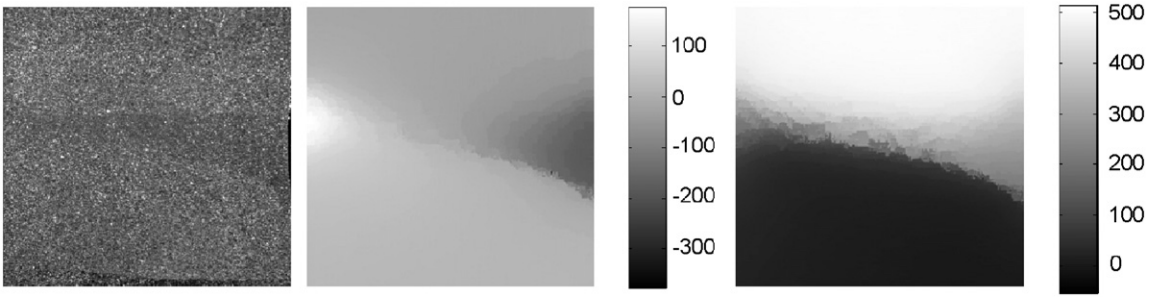

Fig. 13. Displacement fields in microns in *x* and *y* directions respectively of the specimen (schematically presented in Fig. 9) at the beginning of debonding of the film.

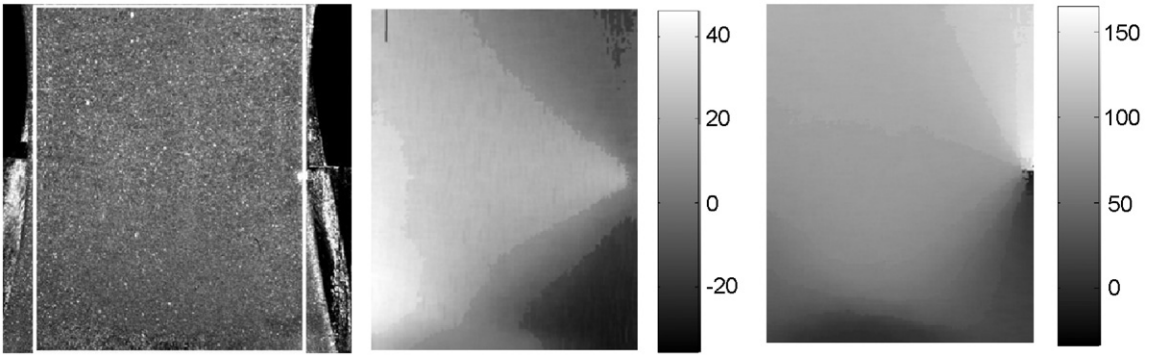

Fig. 14. Displacement fields in microns in *x* and *y* directions respectively of the specimen (schematically presented in Fig. 9) at the beginning of tearing of the front film.

different correlation sub-image windows. This algorithm has been successfully applied to study the notch sensitivity and crack bridging of window security film. The large dynamic range and high accuracy of this algorithm allowed precise experimental analysis of different samples of the investigated material with 0–3 stress concentrators. The processes of the film debonding from the glass surface and the tearing process have also been studied.

The obtained experimental results provide useful information for the theoretical models and numerical simulations of this material. They could also contribute to the further improvement of its mechanical and adhesion properties.

Acknowledgements

This work is supported by the Fund for Scientific Research–Flanders (FWO-Vlaanderen) in the framework of collaboration with the Bulgarian Academy of Sciences, and partially by Grant No. 1521/05-TS, of the BNSF. The authors also greatly acknowledge the support from the NV Bekaert SA Company.

References

[1] Archbold E, Burch JM, Ennos AE. Recording of in-plane surface displacement by double-exposure speckle photography. Opt Acta 1970;17:883–8.
[2] Khetan RP, Chiang FP. Strain analysis by one-beam laser speckle interferometr. 1: single aperture method. Appl Opt 1976;15:2205–15.
[3] Erf RK, editor. Speckle metrology. New York: Academic Press; 1978.
[4] Chiang FP, Khetan RP. Strain analysis by one-beam laser speckle interferometry. 2: multiaperture method. Appl Opt 1979;18:2175–86.
[5] Yamaguchi I. Speckle displacement and decorrelation in the diffraction and image fields for small object deformation. Opt Acta 1981;28:1359–76.
[6] Sirohi RS, editor. Holography and speckle phenomenon and their industrial applications. Singapore: World Scientific; 1988.
[7] Tay CJ, Quan C, Hung YH, Fu Y. Digital image correlation for whole field out-of-plane displacement measurement using single camera. Opt Commun 2005;251:23–36.
[8] Sutton MA, et al. Effect of sub-pixel image restoration digital correlation error estimate. Opt Eng 1988;20:870–7.
[9] Zhang D, Zhang X, Cheng G. Compression strain measurement by digital speckle correction. Exp Mech 1999;39:62–7.
[10] Chu TC, Ranson WF, Sutton MA. Applications of digital-image-correlation techniques to experimental mechanics. Exp Mech 1985;25:232–44.
[11] Bruck HA, McNeil SR, Sutton MA, Peters WH. Digital image correlation using Newton–Raphson method of partial differential correction. Exp Mech 1989;29:261–7.
[12] Hung Po-Chih, Voloshin AS. In-plane strain measurement by digital image correlation. J Braz Soc Mech Sci Eng 2003;25:215–21.
[13] Wattrisse B, Chrysochoos A, Muracciole J-M, Nemoz-Gaillard M. Analysis of strain localization during tensile tests by digital image correlation. Exp Mech 2001;41:29–39.
[14] Zhou P, Goodson KE. Sub-pixel displacement and deformation gradient measurement using digital image/speckle correlation. Opt Eng 2001;40:1613–33.
[15] Zhang J, Jin G. Application of an improved sub-pixel registration algorithm on digital speckle correlation measurement. Opt Laser Tech 2003;35:533–75.
[16] Chen DJ, Chiang FP, Tan YS, Don HS. Digital speckle-displacement measurement using a complex spectrum method. Appl Opt 1993;32:1839–49.
[17] Jin H, Bruck HA. Theoretical development for pointwise digital image correlation. Opt Eng 2005;44:1–14.
[18] Pitter MC, See CW, Somekh MG. Fast sub-pixel digital image correlation using artificial neural networks. Int Conf Image Proc 2001;2:901–5.
[19] Bing P, Hui-min X, Bo-qin H, Fu-long D. Performance of sub-pixel registration algorithms in digital image correlation. Meas Sci Technol 2006;17:1615–21.
[20] Sjodahl M, Benckert LR. Systematic and random errors in electronic speckle photography. Appl Opt 1994;33:7461–71.
[21] Schnars U, Jueptner W. Digital holography, digital hologram recording, numerical reconstruction, and related techniques. Berlin, Heidelberg: Springer; 2005.
[22] Haddadi H, Belhabid S. Use of rigid-body motion for the investigation and estimation of the measurement errors related to digital image correlation technique. Opt Laser Eng 2008;46:185–96.